NJC

PAPER

View Article Online
View Journal | View Issue

Cite this: *New J. Chem.*, 2017, **41**, 11308

Nanostructures prepared *via* laser ablation of tin in water†

Mitsuhiro Honda,[ab] Takahiro Kondo,[a] Tatsuki Owashi,[c] Prabakaran Shankar,[a] Satoru Iwamori,[c] Yo Ichikawa[b] and Sergei A. Kulinich *[a]

Received 15th May 2017,
Accepted 22nd August 2017

DOI: 10.1039/c7nj01634d

rsc.li/njc

In this study, nanomaterials prepared *via* laser ablation of tin in water are systematically studied and compared. Tin targets were ablated by both millisecond and nanosecond pulsed lasers, resulting in core@shell product nanostructures with different chemistries and morphologies. Depending on laser fluence, the obtained core@shell nanoparticles had either Sn or SnO cores and SnO_x shells with varied surface hydration degree. Optical emission spectra of laser-generated plasmas were taken, giving additional support to nanoparticle formation mechanisms. Finally, gas sensing at room temperature is demonstrated as one of the potential applications for such nanostructures.

1. Introduction

Metal oxide nanomaterials have been playing a dominant role in electronics, optoelectronics and photonics.[1–5] Tin oxides are of great interest for both scientific and technological fields owing to their superior chemical and physical properties.[6] Tin exhibits dual valency with oxidation states of (II) and (IV), which allows its oxide nanomaterials to demonstrate different oxygen content, resulting in different electronic structures, for example, with p- and n-type semiconductor characteristics.[7] Of all tin oxide nanomaterials, those based on tin dioxide (SnO_2) are studied better, being considered promising for solid state gas sensors, rechargeable Li-batteries, oxidation catalysts, and optoelectronic devices, photocatalysis, to name several.[8–16] Their performance is dictated by nanostructure sizes, shapes, compositions, and crystal structures, and thus new approaches to produce novel SnO_2-based nanomaterials with controlled morphologies and properties are welcomed and actively investigated.

Laser ablation in liquid (LAL) is an attractive, simple, and efficient method to generate a large variety of nanostructures at a laboratory scale.[15–32] In this approach, a pulsed laser is focused on a solid target (often metal) immersed in liquid and produces nanoparticles (NPs) with various sizes, shapes, compositions and surface chemistry.[19–27,33–35] While a large number of works have been reported on the preparation of ZnO based nanomaterials using LAL,[17,24,26,27,32,35] studies on nanomaterials containing Sn (including tin oxides) prepared by LAL are rather scarce.[15,16,28–31,36]

Tin ablation in pressurized CO_2 was found to generate only metallic Sn NPs.[36] Xiao and coauthors applied LAL to prepare sub-5-nm-sized NPs of $Sn_6O_4(OH)_4$ which exhibited a high photocatalytic activity never observed before in NPs synthesized using conventional methods such as sol–gel or wet-chemistry approaches.[16] Sapkota *et al.* demonstrated a decrease in size of Sn NPs when they were LAL-generated in water in the presence of an electric field.[31] Singh and co-workers claimed the preparation of SnO_2 NPs (smaller than 5 nm) *via* ablating Sn in water,[30] while Musaev and colleagues reported Sn@$Sn(OH)_2$ and SnO_2 NPs as products of LAL in ethanol and water, respectively.[28] Tian *et al.* reported the preparation of Sn NPs in water which then turned to SnO_x upon aging in liquid for several days, the latter NPs being efficient photocatalysts for decaying methylene blue and methyl orange.[15] Finally, Ye and co-workers prepared SnO_x NPs which then were mixed with reduced graphene oxide for further electrochemical applications.[29] In most cases, nanosecond-pulsed lasers were used, and no detailed chemical analysis (especially systematic X-ray photoelectron spectroscopy, XPS) was carried out on the produced NPs, thus leaving the question on the chemical composition of LAL-prepared structures partially open.

This study aimed at ablating Sn in water using different pulse parameters and studying the composition and morphology of the produced NPs. We compare NPs prepared by ablating tin with two different pulsed lasers with same wavelength. The targets were ablated by nanosecond and millisecond pulsed lasers with different pulse width and powers, and the products were carefully characterized by means of structural analysis and spectroscopic techniques. In addition, plasma generated by a millisecond pulsed laser within the ablation zone was evaluated by emission spectroscopy, which allowed for temperature

[a] *Institute of Innovative Science and Technology, Tokai University, Hiratsuka, Kanagawa 259-1292, Japan. E-mail: skulinich@tokai-u.jp*
[b] *Graduate School of Engineering, Nagoya Institute of Technology, Nagoya, Aichi, 466-8555, Japan*
[c] *Department of Mechanical Engineering, Tokai University, Hiratsuka, Kanagawa 259-1292, Japan*

† Electronic supplementary information (ESI) available. See DOI: 10.1039/c7nj01634d

evaluation during NP formation. It is shown that fully oxidized NPs with chemical composition of SnO_2 were never produced, proving rather poor reactivity of metallic tin. In most cases, Sn@SnO_2 core@shell structures were observed. At the same time, SnO@SnO_2 core@shell NPs were found as the product of high-energy millisecond pulses that heat up the ablated spot to temperatures above the boiling point of metallic Sn. Finally, we demonstrate room-temperature gas detection by one of the prepared products as one of the potential applications for such nanomaterials.

2. Experimental

Fig. 1 presents schematic setups used in experiments with nanosecond (ns) and millisecond (ms) pulsed lasers, both being of Nd:YAG type (wavelength 1064 nm). The target was Sn plates (99% purity, 2 mm thick) placed into deionized water. The ns-laser is seen in Fig. 1a to ablate the target vertically through the air/water interface. The amount of water in the vessel was 30 mL and its thickness over the target was 1 cm. The pulse width, pulse power and repetition rate applied were 7 ns, 100–300 mJ per pulse, and 10 Hz, respectively.

The millisecond pulsed laser, as seen in Fig. 1b, irradiated the target through a cuvette side wall. The same setup was previously used to prepare ZnO nanorods and was reported elsewhere.[27] The target plates were placed vertically into a quartz cuvette (30 mm × 30 mm × 50 mm in size, with wall thickness of 2 mm). The amount of liquid used was 15 mL. The laser beam was focused on the target surface by means of a lens with the focal length of 9.0 cm, while its diameter was ~150 μm. The applied pulse peak power was 1 and 5 kW, while the pulse width was changed from 0.5 to 2 ms. This produced pulses with energies from 0.5 to 10 J per pulse (see Table 1). The repetition rate was fixed at 3 Hz for 2 ms and 5 kW (higher energy fluence), while it was 5 Hz for the other conditions. All the samples were prepared in this study for 30 min.

The prepared colloids were drop-cast on Cu grids for further observations by transmission electron microscopy (TEM, HF-2200 from Hitachi). Upon centrifugation (16 500 rpm, 15 min), the separated nanostructures were cast on Si substrates and then characterized by means of XPS (Quantum 2000, ULVAC-PHI) and X-ray diffractometry (XRD, D8 Discover from Bruker). The absorption spectra of fresh as-prepared suspensions were recorded using a UV-vis spectrometer (UV-2450, Shimadzu). Optical emission spectroscopy of the laser-induced plasma was conducted by means of an ICCD camera (iStar from Andor Technology) and a spectrometer (MS257 from Oriel Instruments) which were used to evaluate the temperature inside laser-generated plasma *in situ*. Emission from the laser-induced plasma in water was collected by an optical fiber, then diffracted by the spectrometer and finally detected with the ICCD camera. Because the plasma plume generated by laser beam is very dense and emits continuous spectra, its emission was previously demonstrated to be well described by Planck's law that expresses the spectral density of electromagnetic radiation emitted by a black body in thermal equilibrium at a given temperature T:[37]

$$B(\lambda, T) = \frac{2hc^2}{\lambda^5} \frac{1}{e^{\frac{hc}{\lambda k_B T}} - 1}$$

Here $B(\lambda,T)$ is the spectral radiance of the body (or radiation intensity), λ is the wavelength, h is the Planck constant, k_B is the Boltzmann constant, and c is the speed of light in the medium. Both experimental setup and procedures used for corresponding measurements were similar to those previously reported by Ushida and coauthors.[37]

Table 1 Laser pulse parameters used in experiments with millisecond pulsed laser

Pulse peak energy (kW)	Pulse duration (ms)	Pulse energy (J per pulse)
1	0.5	0.5
1	1.0	1.0
1	2.0	2.0
5	0.5	2.5
5	1.0	5.0
5	2.0	10.0

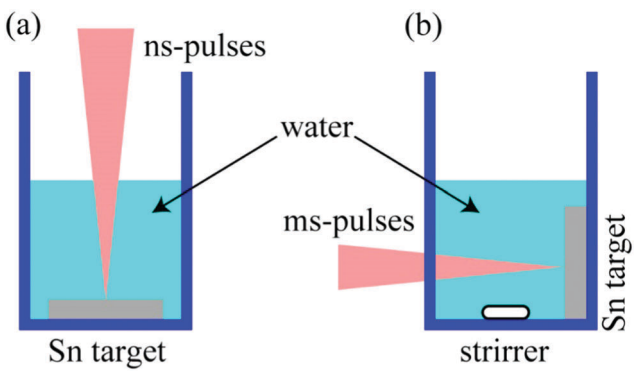

Fig. 1 Experimental setups for laser ablation in liquid using (a) nanosecond and (b) millisecond pulses.

3. Results and discussion

3.1. Morphology and size

All prepared samples were spherical NPs, and no noticeable effect of laser parameters used in this work on their shape and size was observed. When shorter (ns-long) pulses were applied, spherically shaped NPs with sizes mainly smaller than 10 nm were generated, with larger NPs being also present but at smaller numbers. This bimodal size distribution is well known for LAL products and results from all the complexity of NP nucleation, agglomeration and secondary irradiation of already formed NPs with next laser pulses.[19,24,34] No change in NP size or morphology was observed when the power of ns-long pulses was varied from 100 to 300 mJ per pulse. When millisecond pulsed laser was used, the average size of produced NPs mainly remained between ~10 and 25 nm. Fig. S1 (ESI†) shows TEM images of samples prepared by means of ns-(a–c) and ms-pulsed (d–f) lasers. While no experiments were previously reported on Sn-containing NPs prepared by LAL with ms-lasers, the results

observed for ns-laser-generated NPs are generally consistent with those previously reported by others.[15,16,28,30,31] Although in all these studies, ns-lasers with different wavelengths were applied in somewhat different configurations and with somewhat different parameters, in all experiments nanostructures prepared in water and with ns-lasers were spherically shaped NPs of mainly below 10 nm.[15,16,28,30,31] This may be explained by several factors, one being that most Sn-based NPs prepared *via* LAL appear to be nonstoichiometric oxides (SnO_x) or core@shell structures, and often contain a metallic Sn phase, which is believed to prevent them from crystallizing as single-crystal NPs. On the other hand, SnO_2 or SnO-based nanomaterials were not reported as high-surface-energy materials, which is why, unlike the case of ZnO NPs,[27,35] one should not expect strong agglomeration tendency (followed by further recrystallization) from such nanostructures in the absence of surfactants.

The shape of NPs prepared with ms-laser was also spherical (Fig. S1d–f, ESI†), being generally slightly larger than those prepared using ns-laser. Thus far, there have been no reports on the use of ms-lasers for the preparation of Sn-based nanostructures *via* LAL, and below we will show that the chemistry of products prepared by means of such longer pulses is somewhat different. Meanwhile, here it should be mentioned that the majority of NPs observed in Fig. S1 (ESI†) appear to have cores, implying the core@shell structure. This finding will be discussed later, especially in light of strong support from XPS results.

3.2. Phase and chemical composition

Fig. 2a and b show XRD patterns of the products prepared with ns-(a) and ms-long (b) pulses, respectively. Red, blue and black patterns in Fig. 2a correspond to samples prepared with pulse energy of 100, 200 and 300 mJ per pulse, respectively. In Fig. 2b,

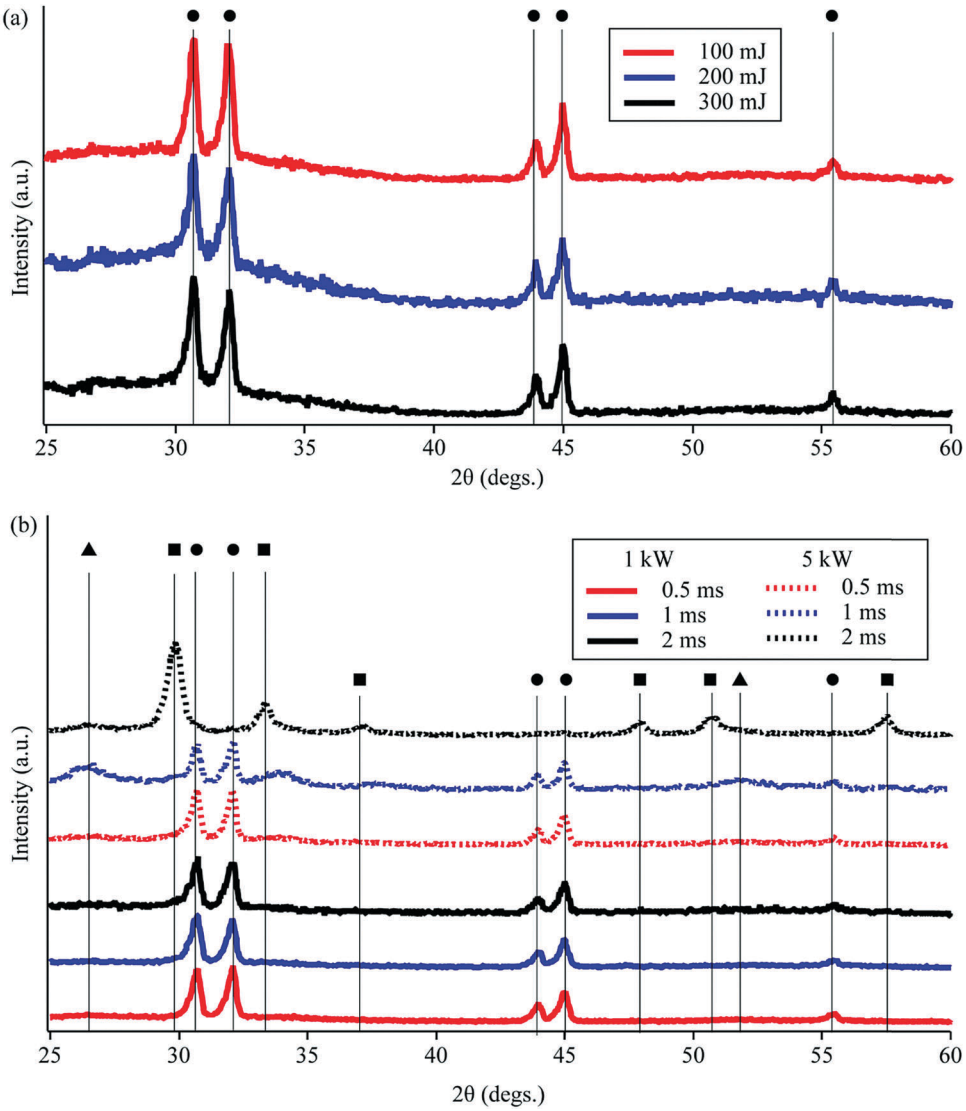

Fig. 2 XRD patterns of products prepared in water using nanosecond (a) and millisecond (b) pulses. In panel (a), red, blue and black colors indicate pulse energies used, 100, 200 and 300 mJ, respectively. In panel (b), solid and dashed lines denote peak powers of 1 and 5 kW, while red, blue and black colors respectively stand for pulse widths, 0.5, 1 and 2 ms. Solid circles, squares and triangles indicate peaks of metallic Sn, SnO and SnO_2, respectively.

colors denote different pulse widths, 0.5 (red), 1 (blue) and 2 ms (black), while solid and dotted lines indicate peak power (1 and 5 kW, respectively) used. Black solid circles, squares and triangles in Fig. 2a and b correspond to peak positions of Sn, SnO and SnO_2 phases, respectively.[38,39] Ablation of Sn target with ns-pulses is seen in Fig. 2a to produce nanostructures containing tetragonal metallic Sn as the main crystalline phase, while no pulse-power influence on phase composition is observed. The appearance of a metallic phase is probably explained by a relatively low reactivity of tin and agrees with some previous work.[31,36,39] Others reported SnO_x or SnO_2 as the main phase in NPs prepared by nanosecond pulsed lasers in water.[15,28,29,30] Later, it will be shown that the NPs whose XRD patterns are exhibited in Fig. 2a have amorphous SnO_2 shells which are not detected by XRD. Similarly, metallic Sn phase is also observed in the majority of samples prepared by ms-pulses, as most of the patterns in Fig. 2b are similar to those in Fig. 2a. However, at higher peak power of 5 kW, when pulse width was raised from 0.5 to 1 ms, peaks of SnO and SnO_2 phases appeared in the XRD pattern (blue dotted line in Fig. 2b). This trend was even more profound when longer pulses of 2 ms were used (black dotted line in Fig. 2b), producing a pattern with a predominantly tetragonal structure of SnO (indicated by solid squares).

Absorption spectra of the as-prepared colloids reveal a certain difference between the products depending on the laser parameters applied (Fig. S2a and b, ESI†). In accordance with the dielectric function, absorption peak of metallic tin is expected at 290 nm, being derived from plasmons of the metallic phase.[40] As well seen in Fig. S2 (ESI†), peaks attributed to metallic Sn are seen in all samples except for the sample prepared using 2 ms-long pulses at 5 kW peak power (black dotted spectrum in Fig. S2b, ESI†). This agrees well with Fig. 2 as the same sample demonstrated no metallic tin in its XRD pattern. The absorption spectra of all suspensions prepared by means of ms-laser are seen in Fig. S2b (ESI†) to have a strong absorption band around 400 nm, thus indicating the formation of oxides SnO_x.[41] At the same time, such a band at 400 nm is not well developed in the case of products prepared with ns-pulses (Fig. S2a, ESI†). Taking into account that Sn is not a highly reactive metal, it is understandable that its oxidation by water during LAL is often incomplete and the metallic Sn phase is detected in obtained NPs, which agrees well with the previous reports of others.[15,31,36] On the other hand, ms-long pulses are known to heat the medium during LAL process,[27] which is expected to stimulate additional oxidation of the formed metallic Sn NPs. In other words, while only a thin SnO_x layer could be formed on the surface of NPs prepared with ns-pulses, core@shell NPs with a thicker SnO_x shell can form during LAL with ms-pulses, thus explaining the broader absorption peaks well observed in Fig. S2b (ESI†). This is supported by temperature measurements after the experiments which demonstrated, respectively, 27 and 35–80 °C in media treated by ns- and ms-pulses. The sample presented by black dotted lines in both Fig. 2 and Fig. S2 (ESI†) (prepared by 2 ms-long pulses with 5 kW as peak pulse power) was oxidized the most, thus demonstrating that using higher energy fluence permits to prepare NPs that are free of metallic tin.

The surface chemistry of all the products was analyzed by XPS, their narrow-scan O 1s and Sn 3d spectra being shown in Fig. 3a, c and b, d, respectively. Panels (a, b) and (c, d) show XPS results for products prepared with ns- and ms-pulses, while line colors correspond to those used in Fig. 2 and Fig. S2 (ESI†). Green, light-blue, gray, and pink peaks are fitting curves denoting O–Sn(IV), O–H, O–C and O–Sn(II) bonding.[15,28,29,42,43] The chemical bonding states in NPs prepared under different conditions are found to be tuned *via* changing laser parameters. Comparison of panels (a) and (c) permits to conclude that while the surface of the products prepared with the ms-laser is densely populated with OH groups (blue fitted curve in Fig. 3c), the contribution of such groups to the spectra in panel (a) is much lower. The use of various pulse widths and peak powers is seen in Fig. 3c and d to provide NPs not only with a higher level of hydroxylation, when compared with ns-laser-prepared NPs, but also with different oxidation states of Sn. It is clearly seen in panel (d) that whereas Sn(II) was well observed in the NPs prepared at lower energy fluence (pulse peak power 1 kW, solid spectra), the use of higher energy fluence (5 kW, dotted spectra) resulted in products with Sn(IV) as the dominant species (see pink and green fitting curves for Sn(II) and Sn(IV), respectively). The sample prepared using ms-pulses at the highest energy fluence (5 kW, 2 ms-long pulses, black dotted spectrum in Fig. 3d), demonstrates practically a pure Sn(IV) peak.

At first glance, the XPS results presented in Fig. 3b and d and those obtained by XRD and absorption spectroscopy (Fig. 2 and Fig. S2, ESI†) somewhat contradict each other. For example, no metallic Sn is seen in Fig. 3b and d, while the metallic phase was a dominant one in the XRD patterns of the majority of samples in Fig. 2, and absorption peaks of metallic Sn were well observed in the UV-vis spectra of the samples (Fig. S2, ESI†). However, this contradiction is easily resolved considering the fact that the probing depth of XPS is just a few nm (no more than 2–3 nm for SnO_2[44]) and assuming that the NPs formed under different conditions are core@shell nanostructures with either metallic Sn or SnO core and SnO_2 shell. In Fig. S3 (ESI†), XPS Sn3d spectra are given for two samples prepared by the ms-laser, both measured as-deposited on the substrate and after ion sputtering. It is well seen that both samples (both prepared at lower fluence: 0.5 ms pulse width and 1 and 5 kW as pulse peak power) demonstrate additional peaks of metallic Sn emerging after the samples were sputtered. This confirms that the NPs prepared in our experiments were indeed core@shell structures, with SnO_2 shells and cores composed of either Sn or SnO phase. Note that this also agrees well with the TEM images presented in Fig. S1 (ESI†).

The scheme in Fig. 4 summarizes the morphology of all nanomaterials prepared in this study under different conditions. The scheme takes into account the results of all the measurements presented above: XRD, UV-vis absorption, and XPS. Importantly, the thickness of the SnO_2 shell is at least $\sim$3 nm, which explains why the chemical bonding of the core was beyond the detection depth of XPS measurements and the spectra shown in Fig. 3 only reveal the chemical composition of the shell. Our results thus permit to conclude that the use of the ns-laser generated

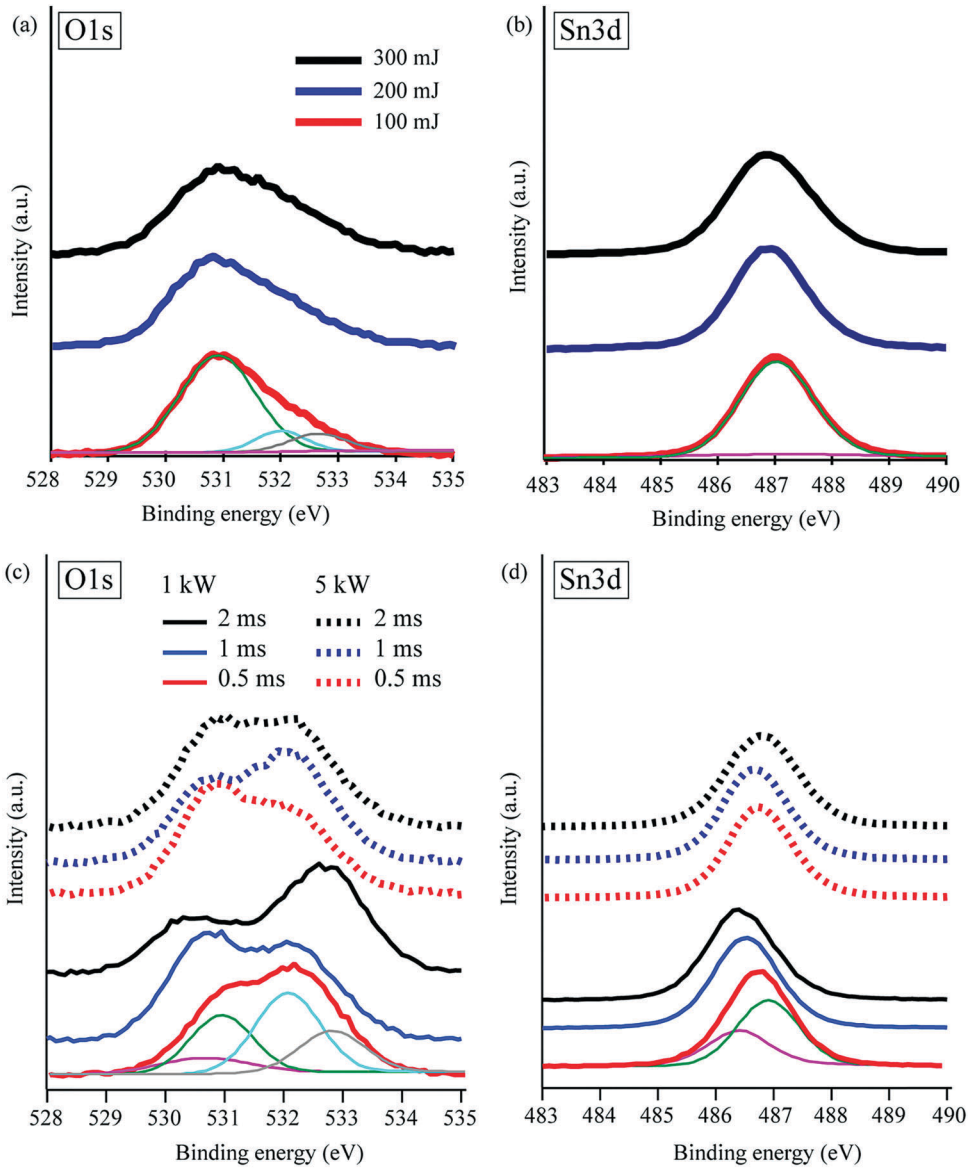

Fig. 3 XPS spectra of products prepared using ns- (a and b) and ms-pulses (c and d). Narrow scans for O1s and Sn3d are presented in panels (a and c) and (b and d), respectively. Red, blue and black spectra shown in (a and b) indicate 100, 200 and 300 mJ per pulse, respectively. In panels (c and d), solid and dotted lines correspond to 1 and 5 kW, while red, blue, and black colors stand for different pulse width, 0.5, 1 and 2 ms. Thin lines in Fig. 3(a–d) are fitting curves denoting O–Sn(IV) (green), O–H (light blue), O–C (gray) and O–Sn(II) (pink) bonding.

$Sn@SnO_2$ NPs, while core@shell nanostructures with either Sn cores (low energy fluence) or SnO cores (higher fluence) and shells of hydrated SnO_2 were formed using ms-pulses (see Fig. 4). Note that $Sn@SnO_x$ core@shell NPs produced by LAL were previously mentioned in the literature[15] while their systematic characterization was not performed.

The obtained results (on core@shell morphology of the product) are in good agreement with previous reports by Niu and coauthors[17,24] who reported NPs with different morphology prepared using ms-laser in liquids with different reactivity. By using liquid media with different oxidizing potential, they reported metal core@oxide (or sulfide) shell nanostructures, hollow NPs, or metal oxide (or sulfide) nanocubes for metals such as Mg and Pb. The formation of core@shell NPs was explained through the formation of metal nanodroplets, followed by surface oxidation that proceeded gradually inward the particle.[17,24] Unlike their systems, the metal ablated in this study, Sn, was less reactive. Furthermore, instead of changing the reactivity of the liquid medium, we changed laser parameters, which in turn changed the reactivity of both liquid and ablated Sn species.

3.3. Optical emission from ablation plasma

To shed more light on the NP formation mechanisms, optical emission spectroscopy was applied to laser-induced plasmas. Fig. 5 presents emission spectra of two plasmas induced by millisecond-long pulses generated under different conditions. Red solid circles and black solid squares indicate spectra recorded

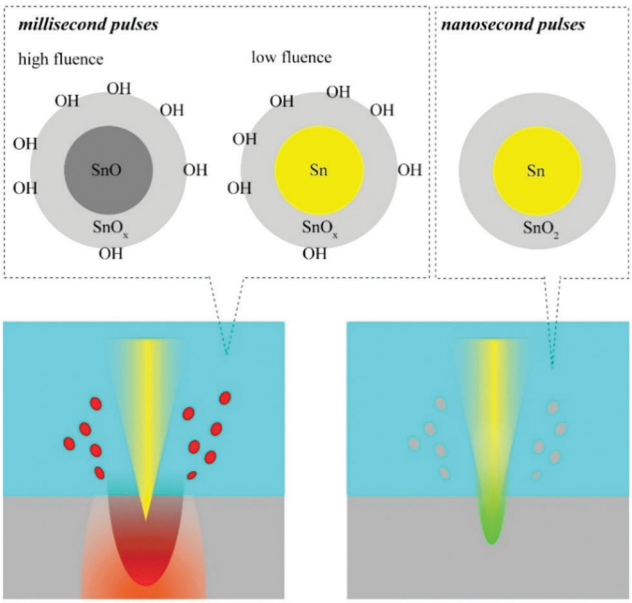

Fig. 4 Schematic presentation of NP morphology obtained with ms- and ns-pulses used.

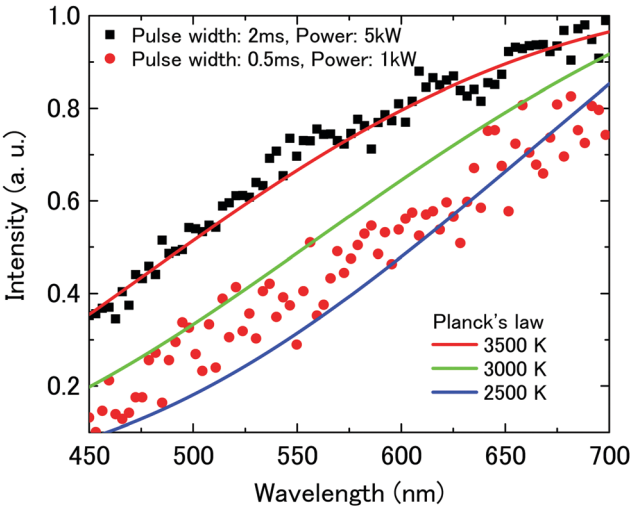

Fig. 5 Emission spectra of ms-laser-induced plasmas measured under different conditions: 2 ms and 5 kW (black squares) and 0.5 ms and 1 kW (red circles). Solid curves indicate calculated spectra based on Planck's law with different temperatures, 3500 (red), 3000 (green), and 2500 K (blue).

at lower energy fluence (1 ms-long pulse width and 1 kW) and higher fluence (2 ms-long pulse width and 5 kW), respectively. Solid curves that are also presented in Fig. 5 show emission spectra calculated based on Planck's law, so that blue, green, and red colors correspond to plasma temperatures of 2500, 3000 and 3500 K, respectively. It is clearly seen in Fig. 5 that the experimentally recorded emissions of plasmas generated at lower laser energy fluence (red circles) and higher energy fluence (black squares) are well consistent with theoretical temperatures of 2500–3000 K and 3500 K, respectively. Importantly, the boiling point of metallic tin is 2875 K, which is above the temperatures created by the lower energy fluence conditions but below those resulting from the higher energy fluence conditions.

During LAL, ablated material is known to be molten and then even vaporized to a vapor or plasma state, depending on the temperature inside the ablation zone.[17,19,24,34] Then in the liquid phase, the material ablated and removed from the target, being in the form of molten droplets, vapor or plasma, reacts with the surrounding medium and NPs form (either around the ablated zone, or inside, or both).[17,19,24,34,39] Because of lower pulse peak energy used, millisecond pulsed lasers were previously reported to produce nanodroplets of molten metal, rather than vapor or plasma of its atoms.[17,24,34] The computation results presented in Fig. 5 by green and blue curves and experimental optical emission data fitting in between the two curves agree well with the above mentioned findings from the literature. This implies that under the condition of lower energy fluence, temperatures were typically below 3000 K, and thus no Sn atoms in vapor or plasma states could be expected in most of our experiments when the ms-laser was exploited. Meanwhile, the emission data recorded for the sample prepared at higher energy fluence (black solid squares in Fig. 5) demonstrate that during this experiment the temperature inside the ablation zone was close to 3500 K, which is obviously larger than the boiling point of the ablated metal (2875 K). As a result, Sn atoms were expected to be evaporated to vapor state, where they could mix with water (and consequently react) with much higher efficiency.

The latter finding may explain why the sample prepared under the conditions whose optical plasma emission is presented in Fig. 5 with black solid squares appears to be more oxidized in its as-prepared form (SnO@SnO$_2$), while the other samples were prepared as Sn@SnO$_2$ NPs (see Fig. 4). It is reasonable to expect lower reactivity when ablated Sn species are (i) not vaporized to vapor or plasma state and (ii) have a lower medium temperature. Under such conditions, their ability to mix and react with water should be lower, which leads to the formation of Sn@SnO$_x$ structures (see Fig. 4).

3.4. Gas sensing toward ethanol

Gas sensing performance of various SnO$_x$ nanomaterials has been reported by many researchers.[12–14,45–48] Nevertheless, gas detection by such materials at room temperature is still unconventional and rare, and nanomaterials working at room temperature are highly anticipated. In this regard, postulating that Sn@SnO$_2$ NPs could be promising for gas sensing, we tested one sample prepared in this study, as this work was not focused on the gas sensing performance of all the prepared nanomaterials. A gas sensing device was prepared by drop-casting a colloid mixture prepared by the ns-laser (at 100 mJ per pulse) onto a commercial inter-digitated electrode. The dynamic response curve recorded for the device in presence of ethanol as a target gas at room temperature is presented in Fig. 6. More details on sample preparation and its detection of other concentrations are presented in the ESI† and in Fig. S4. It is clearly seen in Fig. 6 and Fig. S4 (ESI†) that at room temperature the device could easily detect as little as 50 ppm of ethanol.

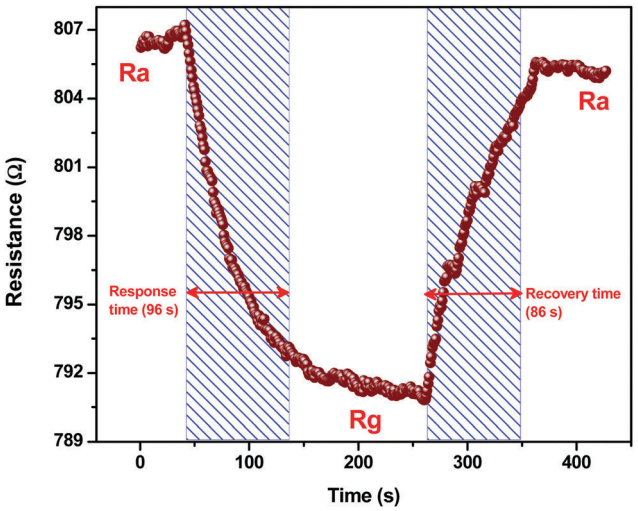

Fig. 6 Response curve of Sn@SnO_2 sample toward 100 ppm of ethanol at room temperature. R_a and R_g indicate the resistance of sensing element in the air and in presence of ethanol (gas), respectively.

For gas sensing, chemiresistive devices are known to use chemical interaction between reducing-gas molecules chemisorbed on the sample surface.[45,46] Normally, such adsorption and desorption of chemical molecules require high thermal activation energy, which is why most of the conventional gas sensors have their working temperatures around 200–300 °C.[45–47] However, LAL-prepared nanomaterials are known for having a high density of surface defects.[19,23–28,34] Such defects are believed to be favorable for gas sorption even at room temperature, which is confirmed by Fig. 6.[47] Further systematic studies are necessary to understand the gas sensing mechanisms of the material tested in this study, for which surface properties such as grain resistance, grain boundary resistance, surface area, and so on should be first evaluated. At the same time, it is believed that the promising result demonstrated in Fig. 6 can be improved upon further optimizing the device, for example, *via* optimizing conditions used to prepare SnO_x-based nanomaterials *via* LAL in different liquid media and probably introducing different dopants.

4. Conclusions

In conclusion, two types of lasers, nanosecond- and millisecond-pulsed lasers, were used to prepare nanomaterials *via* ablating Sn in water, and their products were carefully evaluated. It was found that core@shell nanoparticles of tin-containing materials were produced in all cases. The size of nanoparticles prepared using ns-pulses was mainly below 10 nm, being independent of the pulse energy used and having less hydrated oxide shells compared with their counterparts prepared using ms-laser. When ms-pulses were used, the nanoparticle size was observed to be more dependent of laser parameters, being somewhat larger (up to ~25 nm). At lower laser fluence, metallic cores and SnO_x ($x \sim 2$) shells are found in generated nanoparticles. Meanwhile, at higher energy fluence, ms-laser-ablated Sn species were evaporated in the vicinity of the ablation zone, which led to the formation of a SnO core surrounded by a SnO_2 shell. As a proof-of-concept, a nanomaterial prepared by ns-laser was tested as a gas sensor at room temperature, demonstrating easy ethanol detection at as low level as 50 ppm. It is thus expected that various Sn@SnO_x and SnO@SnO_x nanostructures, with different surface chemistry and sizes, prepared by lasers can find more applications in optoelectronics, gas sensing, and catalysis.

Conflicts of interest

There are no conflicts to declare.

Acknowledgements

The research was financially supported by the Sasakawa Scientific Research Grant from the Japan Science Society (grant 27-221) and the Iketani Science and Technology Foundation (grant 0281031-A). S. A. K. and M. H. are also grateful to the Japan Society for the Promotion of Science (JSPS) for support of this research (grant no. 16K04904 and 15K17431) and to the Daiwa Anglo-Japanese Foundation (Daiwa Foundation Award 11425/12174).

References

1 D. Koziej, A. Lauria and M. Niederberger, Metal oxide particles in materials science: Addressing all length scales, *Adv. Mater.*, 2014, **26**, 235–257.
2 Y. Sun, S. Liu, F. Meng, J. Liu, Z. Jin, L. Kong and J. Liu, Metal oxide nanostructures and their gas sensing properties: A review, *Sensors*, 2012, **12**, 2610–2631.
3 J. C. Manifacier, Thin metallic oxides as transparent conductors, *Thin Solid Films*, 1982, **90**, 297–308.
4 A. Fujishima and K. Honda, Electrochemical photolysis of water at a semiconductor electrode, *Nature*, 1972, **238**, 37–38.
5 S. Lany, Semiconducting transition metal oxides, *J. Phys.: Condens. Matter*, 2015, **27**, 283203.
6 M. Batzill and U. Diebold, The surface and materials science of tin oxide, *Prog. Surf. Sci.*, 2005, **79**, 47–154.
7 Y. Ogo, H. Hiramatsu, K. Nomura, H. Yanagi, T. Kamiya, M. Hirano and H. Hosono, p-Channel thin-film transistor using p-type oxide semiconductor, SnO, *Appl. Phys. Lett.*, 2008, **93**, 032113.
8 A. Kolmakov, Y. Zhang, G. Cheng and M. Moskovits, Detection of CO and O_2 using tin oxide nanowire sensors, *Adv. Mater.*, 2003, **15**, 997–1000.
9 Y. Idota, T. Kubota, A. Matsufuji, Y. Maekawa and T. Miyasaka, Tin-based amorphous oxide: A high-capacity lithium-ion-storage material, *Science*, 1997, **276**, 1395–1397.
10 M. J. Fuller and M. E. Warwick, The catalytic oxidation of carbon monoxide on tin(IV) oxide, *J. Catal.*, 1973, **29**, 441–450.
11 S. Pan and G. Li, Recent progress in p-type doping and optical properties of SnO_2 nanostructures for optoelectronic

device applications, *Recent Pat. Nanotechnol.*, 2011, **5**, 138–161.
12 L. L. Wang, Z. J. Li, L. Luo, C. Z. Zhao, L. P. Kang and D. W. Liu, Methanol sensing properties of honeycomb-like SnO_2 grown on silicon nanoporous pillar array, *J. Alloys Compd.*, 2016, **682**, 170–175.
13 L. F. Zhu, M. G. Wang, T. K. Lam, C. G. Zhang, H. D. Du, B. H. Li and Y. W. Yao, Fast microwave-assisted synthesis of gas-sensing SnO_2 quantum dots with high sensitivity, *Sens. Actuators, B*, 2016, **236**, 646–653.
14 S. H. Li, Z. Chu, F. F. Meng, T. Luo, X. Y. Hu, S. Z. Huang and Z. Jin, Highly sensitive gas sensor based on SnO_2 nanorings for detection of isopropanol, *J. Alloys Compd.*, 2016, **688**, 712–717.
15 Z. Tian, C. Liang, J. Liu, H. Zhang and L. Zhang, Reactive and photocatalytic degradation of various water contaminants by laser ablation-derived SnO_x nanoparticles in liquid, *J. Mater. Chem.*, 2011, **21**, 18242–18247.
16 J. Xiao, Q. L. Wu, P. Liu, Y. Liang, H. B. Li, M. M. Wu and G. W. Yang, Highly stable sub-5 nm $Sn_6O_4(OH)_4$ nanocrystals with ultrahigh activity as advanced photocatalytic materials for photodegradation of methyl orange, *Nanotechnology*, 2014, **25**, 135702.
17 K. Y. Niu, J. Yang, S. A. Kulinich, J. Sun and X. W. Du, Hollow nanoparticles of metal oxides and sulfides: Fast preparation *via* laser ablation in liquid, *Langmuir*, 2010, **26**, 16652–16657.
18 W. J. Qin, S. A. Kulinich, X. B. Yang, J. Sun and X. W. Du, Preparation of semiconductor nanospheres by laser-induced phase separation, *J. Appl. Phys.*, 2009, **106**, 114318.
19 Z. Yan and D. B. Chrisey, Pulsed laser ablation in liquid for micro-/nanostructure generation, *J. Photochem. Photobiol., C*, 2012, **13**, 204–223.
20 T. Kondo, Y. Sato, M. Kinoshita, P. Shankar, N. N. Mintcheva, M. Honda, S. Iwamori and S. A. Kulinich, Room temperature ethanol sensor based on ZnO prepared *via* laser ablation in water, *Jpn. J. Appl. Phys.*, 2017, **56**, 080304.
21 A. I. Savchuk, A. Perrone, A. Lorusso, I. D. Stolyarchuk, O. A. Savchuk and O. A. Shporta, ZnMnO diluted magnetic semiconductor nanoparticles: Synthesis by laser ablation in liquids, optical and magneto-optical properties, *Appl. Surf. Sci.*, 2014, **302**, 205–208.
22 M. H. Mahdieh and B. Fattahi, Size properties of colloidal nanoparticles produced by nanosecond pulsed laser ablation and studying the effects of liquid medium and laser fluence, *Appl. Surf. Sci.*, 2015, **329**, 47–57.
23 N. Tarasenka, A. Butsen, V. Pankov and N. Tarasenko, Structural defects and magnetic properties of gadolinium silicide nanoparticles synthesized by laser ablation technique in liquid, *Phys. Status Solidi B*, 2013, **250**, 809–814.
24 K. Y. Niu, J. Yang, S. A. Kulinich, J. Sun, H. Li and X. W. Du, Morphology control of nanostructures *via* surface reaction of metal nanodroplets, *J. Am. Chem. Soc.*, 2010, **132**, 9814–9819.
25 D. Dorranian, E. Solati and L. Dejam, Photoluminescence of ZnO nanoparticles generated by laser ablation in deionized water, *Appl. Phys. A: Mater. Sci. Process.*, 2012, **109**, 307–314.
26 W. J. Qin, J. Sun, J. Yang and X. W. Du, Control of Cu-doping and optical properties of ZnO quantum dots by laser ablation of composite targets, *Mater. Chem. Phys.*, 2011, **130**, 425–430.
27 M. Honda, T. Goto, T. Owashi, A. G. Rozhin, S. Yamaguchi, T. Ito and S. A. Kulinich, ZnO nanorods prepared *via* ablation of Zn with millisecond laser in liquid media, *Phys. Chem. Chem. Phys.*, 2016, **18**, 23628–23637.
28 O. R. Musaev, M. S. Driver, A. N. Caruso, J. M. Wrobel and M. B. Kruger, Influence of the liquid environment on the products formed from the laser ablation of tin, *Appl. Phys. A: Mater. Sci. Process.*, 2013, **113**, 355–359.
29 Y. Ye, P. Wang, E. Dai, J. Liu, Z. Tian, C. Liang and G. Shao, A novel reduction approach to fabricate quantum-sized SnO_2-conjugated reduced graphene oxide nanocomposites as non-enzymatic glucose sensors, *Phys. Chem. Chem. Phys.*, 2014, **16**, 8801–8807.
30 M. K. Singh, M. C. Mathpal and A. Agarwal, Optical properties of SnO_2 quantum dots synthesized by laser ablation in liquid, *Chem. Phys. Lett.*, 2012, **536**, 87–91.
31 D. Sapkota, Y. Li, O. R. Musaev, J. M. Wrobel and M. B. Kruger, Effect of electric fields on tin nanoparticles prepared by laser ablation in water, *J. Laser Appl.*, 2017, **29**, 012002.
32 T. Goto, M. Honda, S. A. Kulinich, Y. Shimizu and T. Ito, Defects in ZnO nanoparticles laser-ablated in water-ethanol mixtures at different pressures, *Jpn. J. Appl. Phys.*, 2015, **54**, 070305.
33 H. S. Desarkar, P. Kumbhakar and A. K. Mitra, One-step synthesis of Zn/ZnO hollow nanoparticles by the laser ablation in liquid technique, *Laser Phys. Lett.*, 2013, **10**, 055903.
34 H. B. Zeng, X. W. Du, S. C. Singh, S. A. Kulinich, S. K. Yang, J. P. He and W. P. Cai, Nanomaterials *via* laser ablation/irradiation in liquid: A review, *Adv. Funct. Mater.*, 2012, **22**, 1333–1353.
35 S. A. Kulinich, T. Kondo, Y. Shimizu and T. Ito, Pressure effect on ZnO nanoparticles prepared *via* laser ablation in water, *J. Appl. Phys.*, 2013, **113**, 033509.
36 M. Koizumi, S. A. Kulinich, Y. Shimizu and T. Ito, Slow dynamics of ablated zone observed around the density fluctuation ridge of fluid medium, *J. Appl. Phys.*, 2013, **114**, 214301.
37 H. Ushida, N. Takada and K. Sasaki, Diagnostics of liquid–phase laser ablation plasmas by spectroscopic methods, *J. Phys.: Conf. Ser.*, 2007, **59**, 563–566.
38 H. Wang, Y. Wang, J. Xu, H. Yang, C. Lee and A. Rogach, Polyvinylpyrrolidone-assisted ultrasonic synthesis of SnO nanosheets and their use as conformal templates for tin dioxide nanostructures, *Langmuir*, 2012, **28**, 10597–10601.
39 F. Lu, X. Ji, Y. Yang, W. Deng and C. E. Banks, Room temperature ionic liquid assisted well-dispersed core–shell tin nanoparticles through cathodic corrosion, *RSC Adv.*, 2013, **3**, 18791–18793.
40 K. Takeuchi and S. Adachi, Optical properties of β-Sn films, *J. Appl. Phys.*, 2009, **105**, 073520.
41 W. Xia, H. Wang, X. Zeng, J. Han, J. Zhu, M. Zhou and S. Wu, High-efficiency photocatalytic activity of type II SnO/Sn_3O_4 heterostructures *via* interfacial charge transfer, *CrystEngComm*, 2014, **16**, 6841–6847.

42 J. A. Taylor, G. M. Lancaster and J. W. Rabalais, Chemical reactions of N^{2+} ion beams with group IV elements and their oxides, *J. Electron Spectrosc. Relat. Phenom.*, 1978, **13**, 435–444.

43 M. Kwoka, L. Ottaviano, M. Passacantando, S. Santucci, G. Czempik and J. Szuber, XPS study of the surface chemistry of L-CVD SnO_2 thin films after oxidation, *Thin Solid Films*, 2005, **490**, 36–42.

44 K. Nose, A. Y. Suzuki, N. Oda, M. Kamiko and Y. Mitsuda, Oxidation of SnO to SnO_2 thin films in boiling water at atmospheric pressure, *Appl. Phys. Lett.*, 2014, **104**, 091905.

45 J. Tao and M. Batzill, Surface science studies of metal oxide gas sensing materials, in *Metal Oxide Nanomaterials for Chemical Sensors*, ed. M. A. Carpenter, S. Mathur and A. Kolmakov, Springer, New York, NY, 2013, pp. 35–68.

46 M. Batzill, Surface science studies of gas sensing materials: SnO_2, *Sensors*, 2006, **6**, 1345–1366.

47 Z. L. Song, Z. Wei, B. C. Wang, Z. Luo, S. Xu, W. Zhang, H. X. Yu, M. Li, Z. Huang, J. F. Zang, F. Yi and H. Liu, Sensitive room-temperature H_2S gas sensors employing SnO_2 quantum wire/reduced graphene oxide nanocomposites, *Chem. Mater.*, 2016, **28**, 1205–1212.

48 L. L. Wang, L. P. Kang, H. Y. Wang, Z. P. Chen and X. J. Li, Capacitive humidity sensitivity of SnO_2:Sn thin film grown on silicon nanoporous pillar array, *Sens. Actuators, B*, 2016, **229**, 513–519.

